Supporting Information for

Tracking Aqueous Proton Transfer by 2D IR Spectroscopy and *ab initio* Molecular Dynamics Simulations

Rongfeng Yuan,[a†] Joseph A. Napoli,[a†] Chang Yan,[a] Ondrej Marsalek,[b] Thomas E. Markland,[a*] and Michael D. Fayer[a*].
[a]Department of Chemistry, Stanford University, Stanford, California 94305, United States
[b]Charles University, Faculty of Mathematics and Physics, Prague 2, Czech Republic
*tmarkland@stanford.edu; *fayer@stanford.edu
[†]Equal Contribution

This PDF file includes:

Supplementary Text

A. Experimental Section

A1. Sample Preparation and Characterization.

Methyl thiocyanate (97%) (MeSCN) were purchased from Sigma-Aldrich and were used without further purification. Hydrochloric acid (weight percentage 35-37, HCl) was purchased from Fischer Scientific. HCl solutions were prepared by mixing the reagent and the H_2O based on mass to keep the molar ratio between the proton and water molecules to the desired value. MeSCN was added later to the desired concentration, 0.2 mol/L (M) in H_2O, and 0.5-0.6 M in HCl solution.

In HCl solutions, the probe gradually decomposes over time and the half-life of the absorbance was ~12 hrs. The line shape of MeSCN remained the same even though the total absorbance was half the original value and no significant extra absorption were observed elsewhere. All 2D IR measurements were therefore collected within the first 12 hrs of sample preparation.

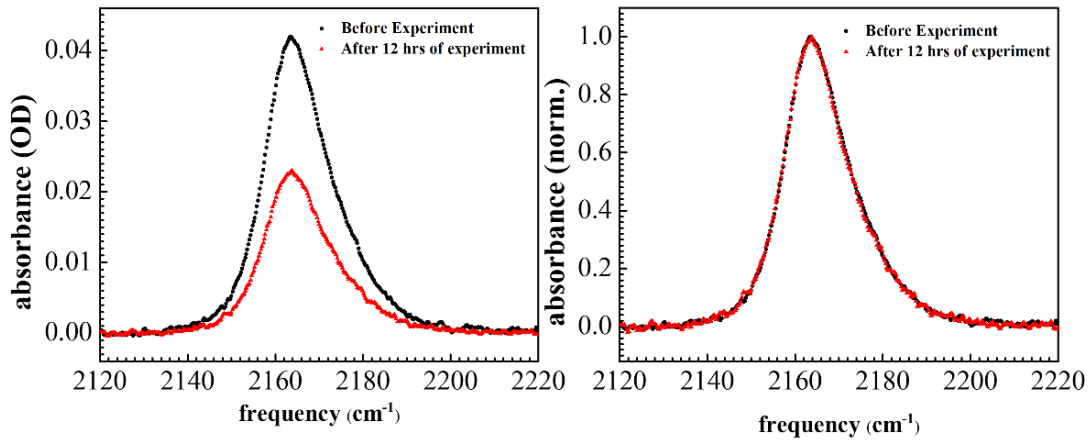

Figure S1. The figure on the left shows the absorption spectra of one sample freshly assembly and after 12hrs of experiment. It showcases the decomposition of MeSCN. On the other hand, the normalized absorption spectra of the two shows the line shape remain the same.

Densities were measured using a 5.00ml pyknometer at room temperature. Kinetic viscosities of the solutions with and without MeSCN were measured using Ubbelohde viscometer at 24 □. Dynamic viscosities were the product between density and kinetic viscosities.

Infrared absorption spectra were measured using a Thermo Scientific Nicolet 6700 FT-IR spectrometer with 0.25 cm^{-1} resolution. Solutions with and without probe MeSCN were measured and scaled subtraction of the two spectra yielded the pure absorption line of the MeSCN in the solutions.

We used the probe concentration of 0.5 to 0.6 M due to high background absorption from hydronium. This is unlikely to affect the experimental results. First, the FTIR absorption spectrum of CN stretch is independent of probe concentration. Second, dynamic viscosity measurement shows a minor ~7 % increase with the addition of the probe (2.01 cP with 0.6M MeSCN vs. 1.85 cP without MeSCN). Finally, ultrafast IR measurements done with 0.3 M and 0.6 M probe lead to the same result within experimental error. Thus, the presence of the probe engenders essentially no dynamical differences in the water network, which is consistent with our earlier work in which we showed that 0.2 M MeSCN in neat water reported the same water dynamics as HOD. This is further supported by the fact that inclusion of the probe molecule in the simulation at a concentration of 0.8 M did not make a statistically significant difference to the simulated self-diffusion constant of the water molecules.

A2. Separation of two components in the MeSCN in HCl solution spectra.

To separate the two heavily overlapped spectral components for MeSCN in HCl solution, we made an approximation that the two individual components remain the same as the HCl

concentration increases from 1:6 to 1:4 (shown in Fig. 1), and the difference of the total spectra among the three concentrations results from the change in relative amplitudes. Then we did scale-subtraction of the 1:6 spectrum from the 1:4 spectrum. The scaling parameter was adjusted so that the resulting hydronium-bonded MeSCN spectrum (H) is symmetric with reasonably flat baseline away from the peak center. This H spectrum was fit to a single Voigt line shape function. Then the original complete spectra of three HCl concentrations were fit with two Voigt functions, with one set of peak parameter fixed to the H component. In this way, the second Voigt peaks (W components) were obtained for all three HCl concentrations. Among the three concentrations, the W peak positions are within 0.6 cm^{-1} and the bandwidths are within 0.5 cm^{-1}. In this way, the H and W component are spectrally separated. The estimated error bars of the peak positions are $\pm$ 0.5 cm^{-1}.

A3. Chemical Exchange Spectroscopy and Its Kinetic Model

Detailed descriptions of 2D IR spectroscopy and Polarization Selective Pump-Probe setup have been presented previously (*20*). Here, we focus on chemical exchange. Chemical exchange occurs when two configurations of the vibrational probe have different absorption frequencies and are in chemical equilibrium. They interconvert without changing the overall number of either species. This phenomenon can only be observed by 2D IR spectroscopy when the interconverting kinetics is fast enough to cause significant changes within the observation window determined by the vibrational lifetime. Chemical exchange spectroscopy (CES) has been applied to multiple systems including the rate of isomerization around a carbon–carbon single bond[1], the switching between well-defined protein structural substates[2], and ion-water hydrogen bond switching(*15*). Chemical exchange has a well-defined effect on the 2D IR spectrum.[3] At T_w short compared to the exchange time constant, the peaks in the IR absorption spectrum corresponding to the 2 species appear as 2 bands on the diagonal of the 2D spectrum. At later T_w, 2 additional off-diagonal peaks grow in due to chemical exchange. In addition, there are 4 going in the negative off-diagonal bands that arise from vibrational echo emission at the 1-2 transition frequencies of each peak, shifted to lower frequencies by the corresponding anharmonicities. All peaks will decay with the vibrational lifetimes.

The evolution of the peaks' volumes is linearly proportional to the corresponding population evolutions, which are analyzed using the kinetic model. In addition to chemical

exchange, the peak volumes are also effected by vibrational relaxation and orientational relaxation.[3,4] To avoid the complication from orientational relaxation, we conducted vibrational echo experiments in parallel and perpendicular polarizations. Here, parallel and perpendicular correspond to pump pulses' polarizations parallel and perpendicular to the probe pulses polarization, respectively. The isotropic signal can be obtained with the weighted average of parallel and perpendicular signal with weight ratio 1:2. The reason for this is clearly shown in Equation 5 in the section A5. In this way, orientational relaxation will not be involved in the fitting routine, thus increasing the robustness of the procedure.

We have reported earlier that MeSCN in concentrated lithium chloride solution has two absorption lines at ~2162 cm^{-1} and ~2179 cm^{-1}.(*20*) The 2162 cm^{-1} peak was assigned to MeSCN population whose nitrogen lone pair forms a hydrogen bond with a water molecule, and the 2179 cm^{-1} line corresponding to MeSCN-Li^{+} complex. We have observed the chemical exchange between the two lines in the 2D spectra. Here we observed similar phenomena between the hydronium-associated (H) and the water-associated (W) components.

At early T_w = 0.6 ps, there are only two diagonal peaks corresponding to the W and H components. At later T_w, for example 18 ps, off-diagonal cross-peaks (WH and HW) have grown in as a result of interconversion between the two complexes. In the context of 2D spectra, all molecules initially in W state, can only be in W or WH state at later T_ws. Hence 2D IR spectroscopy is watching the progression from all the molecules in the W peak (T_w = 0) to the eventual equilibrium between W and WH. Therefore, the populations of W and WH states are related through chemical equilibrium by the exchange rate k_{WH} and k_{HW}. At the same time, they all undergo vibrational relaxation with rate k_W or k_H. To describe these relations, a set of coupled differential equations is required and given below. N_W and N_{WH} corresponding to time dependent populations of the diagonal peak species W and off-diagonal peak species WH, respectively, and the equation is solved with the initial condition $N_{WH}\left(T_w = 0\right) = 0$.

$$\begin{pmatrix} \dot{N}_W \\ \dot{N}_{WH} \end{pmatrix} = \begin{pmatrix} -(k_W + k_{WH}) & k_{HW} \\ k_{WH} & -(k_H + k_{HW}) \end{pmatrix} \begin{pmatrix} N_W \\ N_{WH} \end{pmatrix} \tag{1}$$

where the dot indicates a time derivative. And the solutions are

$$N_W = \frac{N_W(t=0)}{2\Delta}\left[(\Delta+m)\exp\left(-\frac{1}{2}(s+\Delta)t\right)+(\Delta-m)\exp\left(-\frac{1}{2}(s-\Delta)t\right)\right]$$
$$N_{WH} = \frac{N_W(t=0)}{\Delta}k_{WH}\left[-\exp\left(-\frac{1}{2}(s+\Delta)t\right)+\exp\left(-\frac{1}{2}(s-\Delta)t\right)\right] \quad (2)$$

$$s = k_W + k_{WH} + k_{HW} + k_H,$$
$$\Delta = \sqrt{s^2 - 4\left(k_W k_H + k_W k_{HW} + k_H k_{WH}\right)},\ .$$
$$m = k_W + k_{WH} - k_{HW} - k_H$$

Populations of H and HW, N_H and N_{HW}, can be derived following a similar procedure. Besides, chemical equilibrium requires that $N_{WH}(T_w) = N_{HW}(T_w)$ and $N_W(T_w = 0)k_{WH} = N_H(T_w = 0)k_{HW}$. Therefore, there are 3 independent population evolutions, N_W, N_H, and N_{WH}. These evolutions are fitted simultaneously with 1 overall scaling factor and 3 kinetic parameters, k_W, k_H, and k_{WH}.

With the knowledge of the kinetic parameters, the chemical equilibrium independent of the spectroscopic observables is considered. Equation 1 can be modified into Equation 3 for infinite vibrational lifetime. Here N_W and N_H are the populations of W and H species that are in chemical equilibrium.

$$\begin{pmatrix}\dot{N}_W\\ \dot{N}_H\end{pmatrix} = \begin{pmatrix}-k_{WH} & k_{HW}\\ k_{WH} & -k_{HW}\end{pmatrix}\begin{pmatrix}N_W\\ N_H\end{pmatrix} \quad (3)$$

with the initial condition $N_H(t=0) = 0$, the solutions are

$$N_W = \frac{N_W(0)}{s}\left(k_{HW} + k_{WH}\exp(-st)\right)$$
$$N_H = \frac{N_W(0)}{s}\left(k_{WH} - k_{WH}\exp(-st)\right) \quad (4)$$
$$N_W + N_H = N_W(0), s = k_{HW} + k_{WH}$$

These equations describe the relaxation to the chemical equilibrium state if all the molecules were W initially or if a sudden perturbation moved the concentration away from the equilibrium concentrations. For any initial condition, the relaxation time constant is $\tau_{ex} = 1/\left(k_{WH} + k_{HW}\right)$.

Table S1 is a summary of al the fitted parameters and concentrations.

	HCl 1:4	HCl 1:5	HCl 1:6
τ_{WH} (ps)	13.5 ± 2.5	17 ± 3	25 ± 3
τ_{HW} (ps)	7.8 ± 1.5	5.7 ± 1.0	6.0 ± 1.0
τ_{ex} (ps)	4.8 ± 0.5	4.2 ± 0.5	5.0 ± 0.5
k_f ($ns^{-1}M^{-1}$)	4.1 ± 0.8	5.0 ± 0.9	4.4 ± 0.7
k_b ($ns^{-1}M^{-1}$)	7.1 ± 1.3	6.7 ± 1.2	5.2 ± 0.7
$[H_2O]$ (M)	32.3± 0.2	36.1± 0.2	38.9± 0.3
$[H_3O^+]$ (M)	10.8 ± 0.1	9.1 ± 0.1	7.8 ± 0.1

Table S1. Chemical exchange fitting parameters and HCl concentrations. $[H_2O]$ and $[H_3O^+]$ are concentrations of water molecules and hydronium ions, respectively. Unit M stands for mole/L. Note that because one of every four water molecules becomes a hydronium cation, the concentration between $[H_3O^+]$ and $[H_2O]$ is 1:3.

A4. Determination of relative transition dipole moment and equilibrium constant

This method has also been described previously.(*20*) The diagonal peak volumes V_W and V_H are proportional to the fourth power of the corresponding transition dipole moment, i.e., $V_W(t) \propto N_W(t)\mu_W^4$, and $V_H(t) \propto N_H(t)\mu_H^4$. The two off-diagonal peak volumes V_{WH} and V_{HW} are both proportional to $\mu_W^2\mu_H^2$. It is necessary to know the ratio of the two transition dipoles, not their absolute values. The ratio is determined in the following manner. At very early T_w (<1 ps) when exchange is insignificant, the peak volumes are proportional to the equilibrium concentrations. Thus, $V_W(t \approx 0) \propto N_W(t=0)\mu_W^4$ and $V_H(t \approx 0) \propto N_H(t=0)\mu_H^4$. In the linear IR absorption spectrum, the peak areas, S_i, are proportional to the product of the equilibrium concentrations and the transition dipoles squared, i.e., $S_W \propto N_W(t=0)\mu_W^2$ and $S_H \propto N_H(t=0)\mu_H^2$. The two peak areas were obtained from the Voigt fitting shown in Fig. 1. The combination of these data yields the ratios $N_W(t=0)/N_H(t=0)$ and μ_W^2/μ_H^2. The first ratio $N_W(t=0)/N_H(t=0)$ is the concentration ratio of H and W complexes under equal laser pumping. μ_W^2/μ_H^2 is 0.63 ± 0.10 for

HCl solutions and was used to obtain the populations from the peak volumes. These two ratios directly fix the ratio between k_{WH} and k_{HW}, reducing by one dimension the fitting function.

A5. Polarization Selective 2D IR Spectroscopy and the determination of reorientational relaxation

In a system involving chemical exchange, simply doing Polarization Selective Pump-Probe (PSPP)[5,6] is not enough to extract the orientational dynamics of the two species because chemical exchange mixes the two lifetimes and orientational relaxation times. To disentangle the orientational dynamics from the chemical exchange, polarization selective 2D IR was used. The setup is the same as the PSPP setup in a previous publication. [6]Pump and probe polarizers are set to be 45° relative to horizontal and horizontal, respectively. A computer-controlled resolving polarizer switches between the horizontal and vertical position to acquire data for parallel and perpendicular fashion. Thus the 2D IR signals in the parallel and perpendicular configurations were measured at the same time. The effect of polarization control in 2D IR CES experiments has been described previously[3,4] and we presented the final results (Equation 5) that describe the population evolutions of diagonal and off-diagonal peaks under parallel and perpendicular configurations. Here k_W, k_H, k_{WH} and k_{HW} have the same meaning as in Equation 1 and 2. D_W and D_H are the orientational diffusion constants for species W and H, respectively. Note that Equation 5 assumes that the reorientational relaxation of both species is single exponential without wobbling-in-a-cone behavior. For the systems discussed here, this assumption works well as will be shown below.

$$
\begin{aligned}
&\begin{pmatrix} N_W(T_w) \\ N_{WH}(T_w) \end{pmatrix}_{para} = \left(e^{R\cdot T_w} + \frac{4}{5} e^{S\cdot T_w} \right) \times \frac{1}{3} \begin{pmatrix} N_W(0) \\ N_{WH}(0) \end{pmatrix}_{para} \\
&\begin{pmatrix} N_W(T_w) \\ N_{WH}(T_w) \end{pmatrix}_{perp} = \left(e^{R\cdot T_w} - \frac{2}{5} e^{S\cdot T_w} \right) \times \frac{1}{3} \begin{pmatrix} N_W(0) \\ N_{WH}(0) \end{pmatrix}_{perp} \\
&R = \begin{pmatrix} -(k_W + k_{WH}) & k_{HW} \\ k_{WH} & -(k_H + k_{HW}) \end{pmatrix} \\
&S = \begin{pmatrix} -(k_W + k_{WH} + 6D_W) & k_{HW} \\ k_{WH} & -(k_H + k_{HW} + 6D_H) \end{pmatrix}
\end{aligned}
\tag{5}
$$

Both the parallel and perpendicular 2D IR spectra time dependence can be characterized in terms of two diagonal peaks and one off-diagonal peak, and overall there are 6 independent

peak volume evolution curves. k_W , k_H , k_{WH} and k_{HW} have already been obtained by the procedure described in Section 2 and are fixed here. D_W, D_H and an overall scaling factor are the only variables to fit the 6 curves simultaneously. The peak volume data (points) and the fitted curves (solid curves) are shown Figure S2 for the HCl:H_2O molar ratio of 1:4. The model reproduces the polarization selective data exceptionally well. Considering the experimental error, the fitting result shows no discernable difference in reorientational relaxation between the H and W component and the time constant is 5.9 ± 0.4 ps.

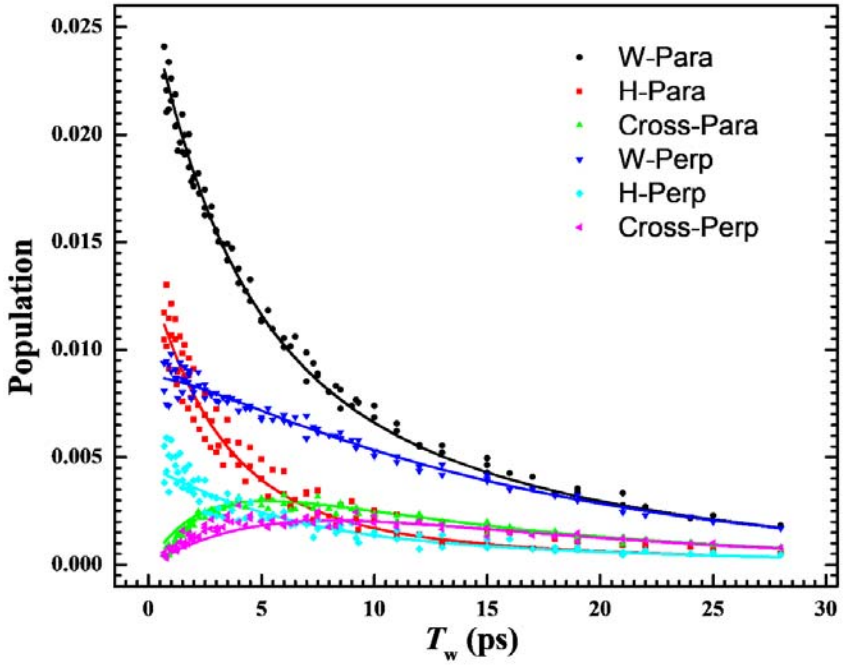

Fig. S2. This figure shows the experimental population data versus the fit using the kinetic model described above. Note that this figure plots the population, which derives from peak volume with proper transition dipole corrections. In the legend, W and H corresponds to the diagonal peak of water- and hydronium- associated component. "Cross" corresponds the cross peak of H and W component. The suffix -para or -perp indicates the experimental polarization geometry.

A6. Heating Background Subtraction method

A previous article has explicated this issue.(*20*) IR pulses can cause temperature increases in the sample. Some molecule's infrared absorption spectra can be shifted due to temperature increase. Therefore, a heating signal arises from the IR absorption spectra difference between pump pulses "on" and "off", and this signal interferes with the analysis of resonant signal. The heating signal usually grows with the vibrational relaxation lifetime as the excited states deposit energy into the bath, increasing the overall temperature of the surroundings.

Water and aqueous solutions have significant IR absorption over a wide range of infrared frequencies, which can produce time dependent heating signals. This was observed very early when HOD was used as a vibrational probe to examine hydrogen bond dynamics.[7,8] We would like to reiterate the conclusion of the paper mentioned above that there are two sources of background signal. One source of background is from water and hydronium absorption. They basically added a slowly varying offset to the whole 2D spectra, which is in sharp contrast to the highly structured resonance signal with very narrow line widths. The second source is the heating signal from the probe MeSCN, which causes similar background to the LiCl solution. It is weak but highly structured. These signals have positive and negative going features, some of which overlap the MeSCN 2D spectra. These structured heating peaks are so weak that they cannot be observed at the earlier T_ws because of the strong resonant signals but are not insignificant at the longer T_ws.

To obtain the time dependence of the growth of the broad signal, PPSP experiments were first conducted on a background sample without MeSCN to measure the rate of increase of the heating signals. The example of HCl 1:4 H2O solution is presented in Fig. S3 A. The growth of heating signal was fit with a biexponential function with time constants 0.8 ps and 3.2 ps. These values barely changed across the HCl concentration range. Then, probe and background samples were measured at the same series of waiting times, T_w, as used in the vibrational echo experiments. At T_w = 250 ps when no resonant signal is left and the heating signal is constant, the signal of the background sample (originating from the first source) was scale-subtracted from the real sample so that the region of the higher ω_m frequencies 2190 cm^{-1} to 2220 cm^{-1} had no signal. Then 2D spectra at other T_ws were processed using the same scaling factor.

Next, to remove the more structured heating features, they were observed at a very long T_w, usually 250 ps. 250 ps is longer than 10 times the CN stretch lifetime in HCl solution, so the resonant signal has decayed to zero, and the heating signal is constant. It was assumed that the very weak structured heating features grow in at the same rate as the broad feature. This is a reasonable assumption because the proton background has a broad absorption with about ~ 1 OD amplitude while the probe only has an absorption of ~ 50 mOD and the line width is very small. Overall, hydronium/water vibrational modes absorb most of the energy and the temperature rise should be caused by the hydronium/water absorption. An exponential growth model of 2D spectra heating background, with time constants from the pump-probe measurement and final amplitudes from the long T_w 2D measurements were used to subtract the heat induced signals.

The second part of the heating signal is relatively small. The procedure is robust because a small error in subtraction of a small signal does not affect the results presented in the main text. The two panels of Figure S3 B show the magnitude of heating signal compared to the overall signal obtained at 5.3 ps. Overall, the background signal is small and relatively flat compared to the highly structured resonance signal.

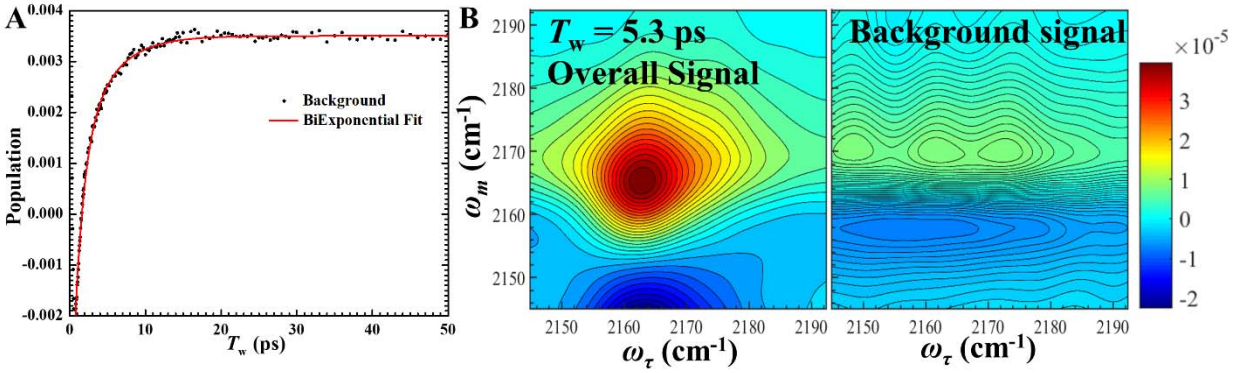

Figure S3. **A** represents the growth of heating signal measured by pump-probe in the background sample HCl 1:4 H_2O solution without the probe MeSCN. The red line is the biexponential fit to the data. The two panels of **B** show the magnitude comparison between the overall signal and heating signal in isotropic polarization setting at 5.3 ps in HCl 1:4 H_2O solution. The first panel is the 2D spectrum obtained directly from experiments, including both resonance and background signals. The background signal spectrum includes contribution from both water and the probe. The two spectra share the same color map that is shown on the right.

A7. Use 2D Gaussians to model 2D spectra, shown in Fig. 2

As was mentioned in the main text, we used a 2D Gaussian function to model one band in the 2D spectra and several 2D Gaussians to model a full 2D spectrum. The result is shown in the second row of Fig. 2. In order to show that the extra peaks are indeed exchange peaks labelled on the 2D spectra at 25 ps, we use the 2D Gaussians that describes the diagonal populations (W & H, including 0-1 and 1-2 transition) and adjust their relative peak volume solely based on the propagation of vibrational relaxation at 0.6 ps and 25 ps without the effect of chemical exchange. These 2D spectra were shown on the third row of Fig. 3. Comparison of three rows of 2D spectra shows that the extra peaks in the 2D spectra are exchange peaks.

A8. Spectral diffusion of W component in 2D spectra

We used the Center Line Slope (CLS)[9,10] method to quantify the band shape change in 2D spectra and thus spectral diffusion or Frequency Frequency Correlation Function (FFCF). However, for 2D spectra with overlapping IR absorption bands, directly applying this method will not yield the correct CLS or FFCF values. Previously, several methods have been developed to

treat these challenging situations.[11,12] Based on the general idea of isolating the bands, we've developed a new method to better suit the need of the current system. As was mentioned in section A7, we have used the 2D Gaussian functions to model 2D spectra. To examine the diagonal W peak, we subtracted other peaks from 2D spectra using their 2D Gaussian functions. In this way, the diagonal W band shape is free from the interference from other peaks. A more detailed description of this method will be presented in a publication later.

B. Simulation Section

B1. Ab initio molecular dynamics simulations details

We performed classical *ab initio* molecular dynamics (AIMD) simulations of a molecule of methyl thiocyanate (MeSCN) in neat water and concentrated hydrochloric acid in the NVT ensemble at T = 300 K under periodic boundary conditions. The GGA level of density functional theory (DFT) was used to describe the electronic structure of the system. Simulations were performed using the i-PI program[13,14] and employed a multiple timescale (MTS) integrator of the r-RESPA form[15].

Initial configurations for the AIMD simulations were obtained using a 3-step procedure: (i.) construction and initial equilibration via force field-based MD (FFMD) simulations, (ii.) equilibration in the NPT ensemble on the DFT potential energy surface (PES) to establish the density of the aqueous HCl system, and (iii.) production in the NVT ensemble on the DFT PES to generate dynamics. We detail each step below.

Initial configurations for the FFMD simulations were first obtained. For the simulation of MeSCN in neat water, the initial configuration was obtained by solvating one gas-phase MeSCN molecule with 118 water molecules using OpenMM's Modeller class, specifying a padding distance of 6.5 Angstroms. For MeSCN in aqueous HCl, one of the MM-equilibrated configurations of MeSCN in neat water was selected and 23 water molecules were replaced by chloride anions at random.

For these initial FFMD equilibration simulations, parameters for the MeSCN molecule were obtained from the Generalized Amber Force Field [16,17], parameters for aqueous chloride ions were obtained from Dang et al [18], and the TIP4PFB force field [19] was used for the water molecules. The Lorentz-Berthelot (arithmetic) combining rule was employed in computing the non-bonded interactions between atom types specified by different force fields. We used the

OpenMM [20-23]software package to perform these simulations, which were run under NPT conditions at T = 300 K and P = 1 atm and employed a Langevin Thermostat (with a time step of 0.5 fs and friction coefficient of 0.5 ps^{-1}) and Monte Carlo Barostat (with a spacing of 25 MD steps between volume scaling attempts). FFMD simulations were run for 20 ns, from which 4 configurations were extracted spaced in time by 5 ns. These configurations were then further equilibrated as follows.

For the MeSCN in HCl simulations, for each of the 4 starting configurations taken from the FFMD simulations, 23 randomly selected water molecules were protonated in order to obtain a system of net neutral charge and a water molecule to HCl pair ratio of 95:23 (~1:4) so as to match experiment. This corresponds to an HCl concentration of 9.8 M. We then minimized the positions of all hydrogen atoms on the DFT PES (further details about the DFT PES below) in order to quench the excess energy introduced upon switching from the FF PES to the *ab initio* PES as well as the introduction of strain in the hydrogen bond network upon randomly protonating water molecules . Hydrogen positions were minimized for MeSCN in neat water as well. AIMD simulations of MeSCN in neat water were run at the average density obtained from the initial 20 ns FFMD equilibration run (ρ = 0.999 g / cm3). For the simulations of MeSCN in concentrated solution we performed a further AIMD NPT equilibration as described below to obtain the density.

Additional AIMD NPT runs were performed in order to establish the density of MeSCN in aqueous HCl. Uncorrelated FFMD configurations were used as initial configurations for these simulations. These NPT simulations were run directly in CP2K employing the parameters detailed below, but with a larger cutoff of 800 Ry used. This cutoff has previously been shown to produce converged results for liquid water [24]These simulations employed a time step of 0.5 fs, massive Nose-Hoover thermostats to enforce a temperature of T = 300 K, and a barostat enforcing a pressure of P = 1 atm with a time constant of 200 fs. This setup was confirmed to give a density for neat liquid water that was consistent with previously published results. For MeSCN in the 9.8 M HCl solution an average density of ρ = 1.127 g cm^{-3} was obtained from an aggregate of ~50 ps of simulations, split into 4 trajectories of equal length. (see Figure S4)

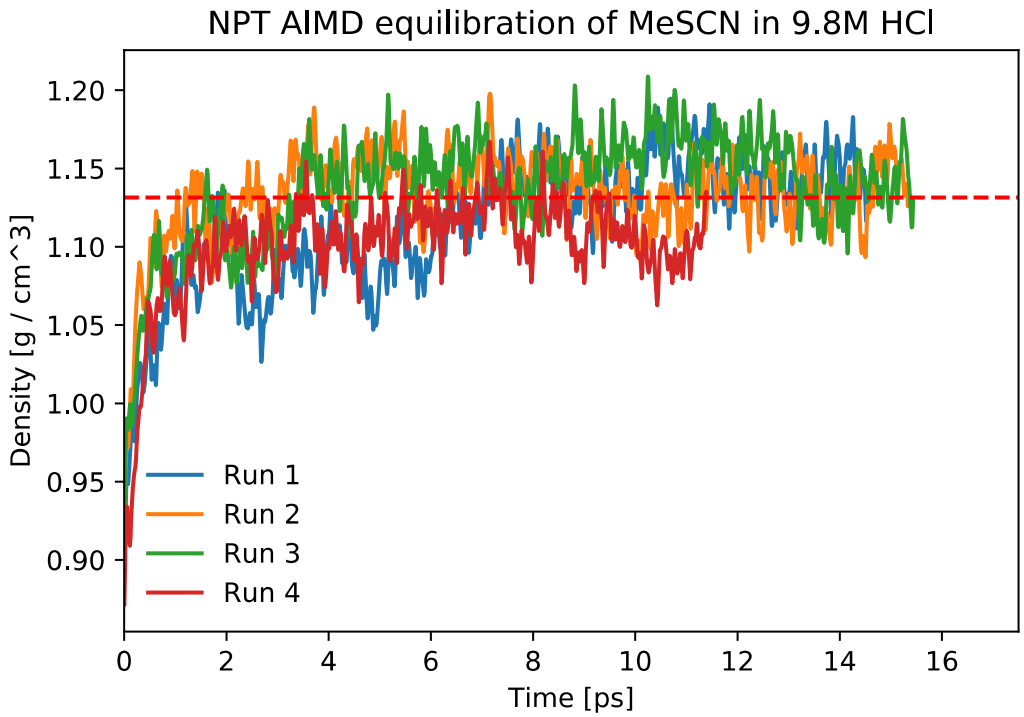

Fig. S4. NPT AIMD equilibration trajectories for MeSCN in 9.8M HCl. Each trajectory shows an initial density increase and then plateaus, fluctuating around densities between 1.10 and 1.18 g cm^{-3}. The final density used for the simulations of MeSCN HCl of 1.127 g cm^{-3} was obtained from the four trajectories as the average density between 3 and 16 ps.

Hydrogen position optimization, AIMD NPT equilibration, and full forces for MTS production runs were evaluated using the CP2K program[25,26] at the DFT level of electronic structure theory using the revPBE[27,28] GGA functional, with D3 dispersion corrections[29] added. Atomic cores were represented using the dual-space Goedecker-Tetter-Hutter pseudopotentials[30]. Within the GPW method[31], Kohn-Sham orbitals were expanded in the TZV2P basis set, while an auxiliary plane-wave basis with a cutoff of 400 Ry was used to represent the density. The self-consistent field cycle was converged to an electronic gradient tolerance of $\varepsilon = 5 \times 10\text{-}7$ using the orbital transformation method[32] with the initial guess provided by the always-stable predictor-corrector extrapolation method[33,34] at each MD step.

The AIMD MTS[35,36] simulations of MeSCN in HCl solution and neat water employed a 2.0 fs outer time step and a 0.5 fs inner time step. Full forces were evaluated using the CP2K program as described above. MTS reference forces were evaluated at the SCC-DFTB3[37] level of

theory using the DFTB+ program[38]. The 3ob parameter set[39] was used and dispersion was included via a Lennard-Jones potential[40] with parameters taken from the Universal Force Field[41].

In aggregate, we simulated 1695 ps and 1832 ps of trajectory of the MeSCN probe in aqueous HCl and neat water solutions, respectively. For MeSCN in neat water, we initially ran ~340 ps of trajectory starting from the four uncorrelated initial configurations described above. We then sampled a set of 20 frames, each spaced by 15 ps, from this 340 ps of trajectory and launched additional 20 ps trajectories, resampling atomic velocities from the Maxwell-Boltzmann distribution in order to more efficiently sample the vibrational modes of the C-N stretch (This mode is strongly decoupled from the rest of the system due to being almost harmonic and spectrally well separated from other system modes. This is why it is a good vibrational probe due to its long vibrational lifetime, but also results in non-ergodic behavior in the simulation). Similarly, for MeSCN in 9.8 M HCl, we initially performed ~680 ps of trajectory. We then sampled a set of 20 frames, each spaced by 15 ps, from this trajectory and launched additional 20 ps trajectories, resampling atomic velocities from the Maxwell-Boltzmann distribution.

B2. Orientational relaxation of MeSCN in neat water and 9.8 M HCl

The orientation relaxation of the MeSCN probe in neat water and in 9.8 M HCl was analyzed in a way similar to previous work[42]. Second-order orientation correlation functions were calculated using the C-N unit displacement vector across the trajectories. Orientation relaxation times were then extracted by performing bi-exponential fits of the resulting correlation functions between 0 and 10 ps. Below in Fig. S5 and S6, we show the anisotropy of MeSCN in water and in 9.8 M HCl, with the experimental result shown for MeSCN in water for comparison.

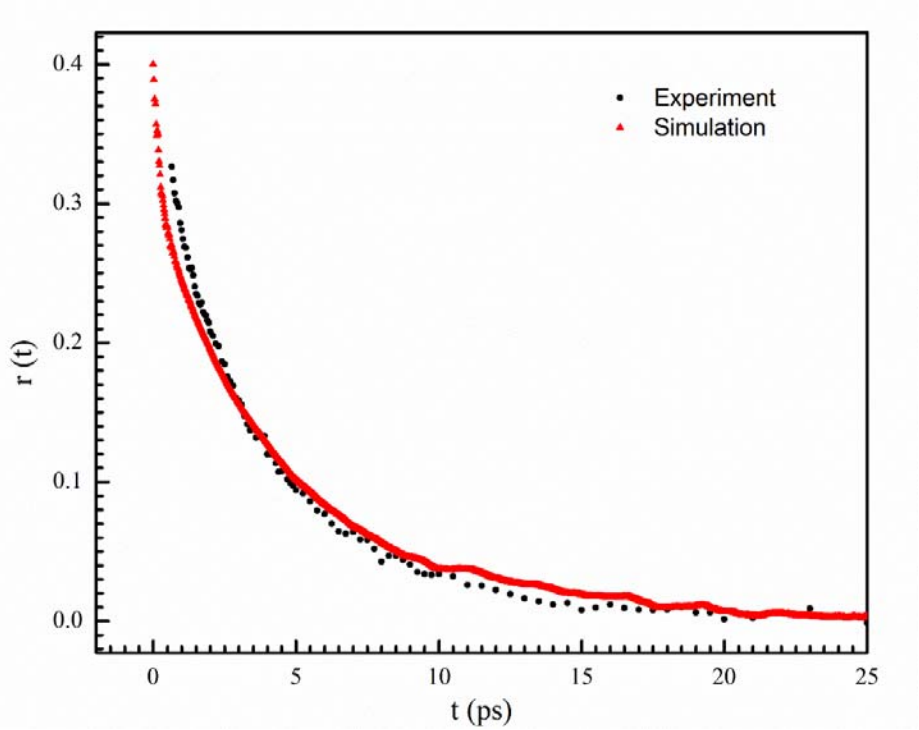

Fig. S5. The anisotropy r(t) of MeSCN in neat water is extracted from simulation as the second-order orientation correlation of the C-N unit displacement vector. Experimental data is displayed for comparison. Fitting the simulation result to a bi-exponential function between 0 and 10 ps yields a reorientation timescale of 4.8 ps.

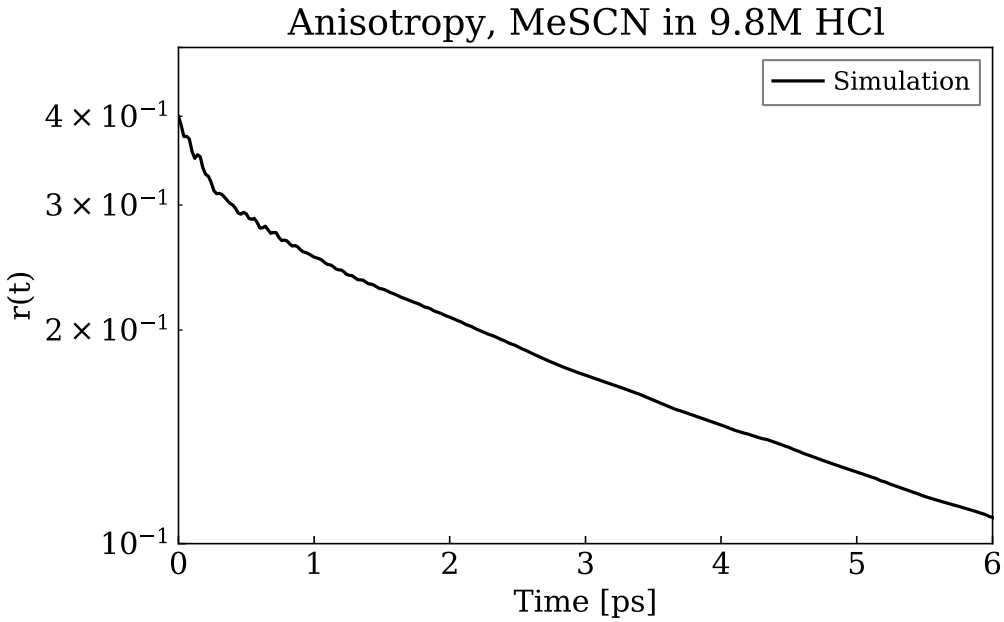

Figure S6. The anisotropy of MeSCN in 9.8 M HCl is extracted from simulation as the second-order orientation correlation of the C-N unit displacement vector. The lighter curves are individual simulation trajectories and the solid black curve is the average. Fitting the simulation result to a bi-exponential function between 0 and 10 ps yields a reorientation timescale of 6.4 ps.

B3. Identification of H* atoms that form part of hydronium molecules

In the main text, we present results that rely on identifying hydrogen atoms that belong to proton defects (which we refer to as H* atoms) in each frame of the trajectory. In order to identify these atoms, we use a nearest-neighbor criterion and assign each hydrogen atom to the closest oxygen atom. H* atoms are then identified as belonging to triply-coordinated oxygen atoms (O*).

B4. Obtaining the time-dependent CN vibrational spectrum and defining the hydronium-bound MeSCN state

In the main text, we present the linear vibrational spectrum of the CN stretch of MeSCN. In order to correlate the vibrational motion of the CN stretch of the MeSCN probe with structural features of the HCl solution, we computed the time-dependent vibrational density of states (VDOS) for the CN stretch, an approach that has been detailed in our previous work[43,44]. Here, in order to isolate the CN stretching mode of MeSCN, we first computed the relative velocity between the C and N atoms of the CN group across the simulation trajectory. This relative velocity was then projected onto the C-N unit displacement vector. The time-dependent VDOS of the CN stretch was then obtained using this projected relative velocity. We employed the symmetric Hann windowing function with a full end-to-end width of 4 ps and extracted the instantaneous frequency of the CN stretch as a weighted average over the frequency interval 1510-2810 cm^{-1}.

In order to identify the hydronium-bound state, we first identified all H* atoms in each frame of the simulation, as detailed above. MeSCN was identified to be bound to hydronium if any H* in the system was within 2.25 Angstroms of the MeSCN nitrogen atom. As shown in Fig. S6, this distance corresponds to the first minimum in the N-H* radial distribution function (RDF).

B5. N-H* radial distribution function

As referred to in the main text, the joint probability distribution of the CN stretch frequency and the distance of the closest H atom of a hydronium (H*) to the N exhibits peaks that coincide with the first and second peaks in the N-H* RDF. The N-H* RDF calculated from our trajectories of MeSCN in 9.8 M HCl is provided below in Fig. S7.

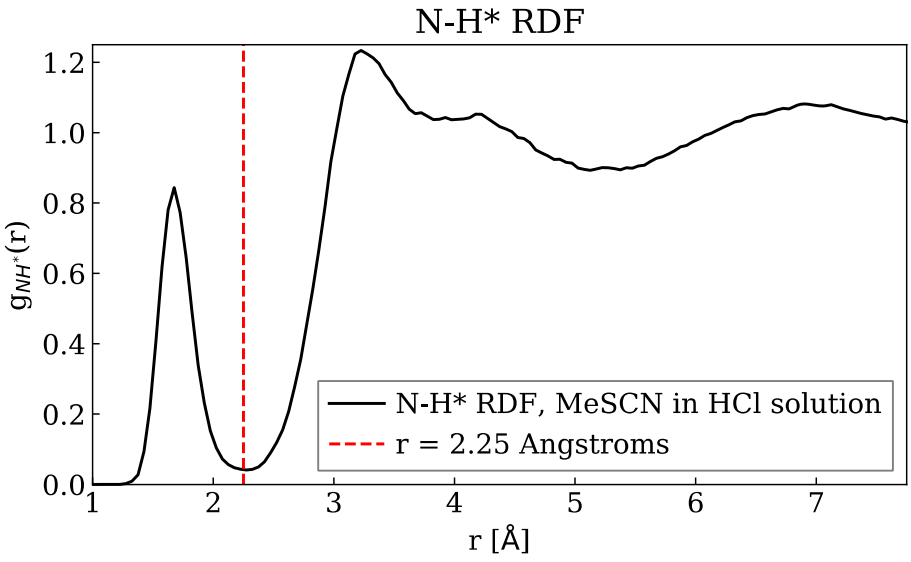

Figure S7. N-H* radial distribution function extracted from simulations of MeSCN in 9.8 M HCl. The vertical dotted red line indicates the distance cutoff used to determine whether the MeSCN is in the hydronium-bound state.

B6. Free energy difference between the H_2O and H_3O^+ bound states

In the main text, we refer to the difference in the free energy between the water and acid bound states relative to experiment of 0.5 kcal mol^{-1} which is obtained as follows. The MeSCN is bound to hydronium 20% of the time in the simulations and 36% of the time in the experiment. We thus can obtain the free energy difference between the hydronium-bound and water-bound states for simulation as,

$$\Delta A_{sim} = -k_B T \ln\left(\frac{0.20}{0.80}\right) = 0.83 \text{ kcal} \cdot \text{mol}^{-1}$$

where $k_B T = 0.596 \text{ kcal} \cdot \text{mol}^{-1}$ at T = 300 K. For the experiment, we also compute the difference in free energy as,

$$\Delta A_{\text{exp}} = -k_B T \ln\left(\frac{0.36}{0.64}\right) = 0.34 \text{ kcal} \cdot \text{mol}^{-1}$$

The difference between simulation and experiment is then obtained as:

$$\Delta\Delta A = \Delta A_{sim} - \Delta A_{\text{exp}} = 0.49 \text{ kcal} \cdot \text{mol}^{-1}$$

B7. Extracting the hydronium-water exchange rate constant

The 2.2 ps exchange time scale in the main text was extracted from the simulations for hydronium-water exchange near MeSCN as follows. As detailed above, MeSCN is defined as being hydronium-bound if any H* in the system is within 2.25 Angstroms of the MeSCN nitrogen atom and is defined as water-bound otherwise. Hence using the Heaviside function, h, and defining the smallest N-H* distance in the system as R_{NH^*}, the reaction coordinate is defined as $h(t) = h\left(2.25\text{Å} - R_{\mathrm{NH}^*}(t)\right)$. The time constant for the hydronium water exchange process, $\tau_{eq} = \left(k_{HW} + k_{WH}\right)^{-1}$, can then be extracted from the long-time exponential decay of the normalized side-side correlation function[45],

$$C(t) = e^{-t/\tau_{eq}} = \frac{\langle \delta h(0)\delta h(t)\rangle}{\langle \delta h(0)\delta h(0)\rangle} = \frac{\langle h(0)h(t)\rangle - \langle h\rangle^2}{\langle h^2\rangle - \langle h\rangle^2} = \frac{\langle h(0)h(t)\rangle - \langle h\rangle^2}{\langle h\rangle - \langle h\rangle^2}$$

where $\delta h(t) = h(t) - \langle h\rangle$ and the last equality follows since h can only take values 1 and 0 and hence $\langle h^2\rangle = \langle h\rangle$. Here one can note that $\langle h\rangle$ is the proportion of the simulation time MeSCN is bound to hydronium and $1 - \langle h\rangle$ is the proportion of time it is bound to water. We extracted the time constant by performing a linear fit to ln[$C(t)$] between 1 and 3 ps, shown in Fig. S8.

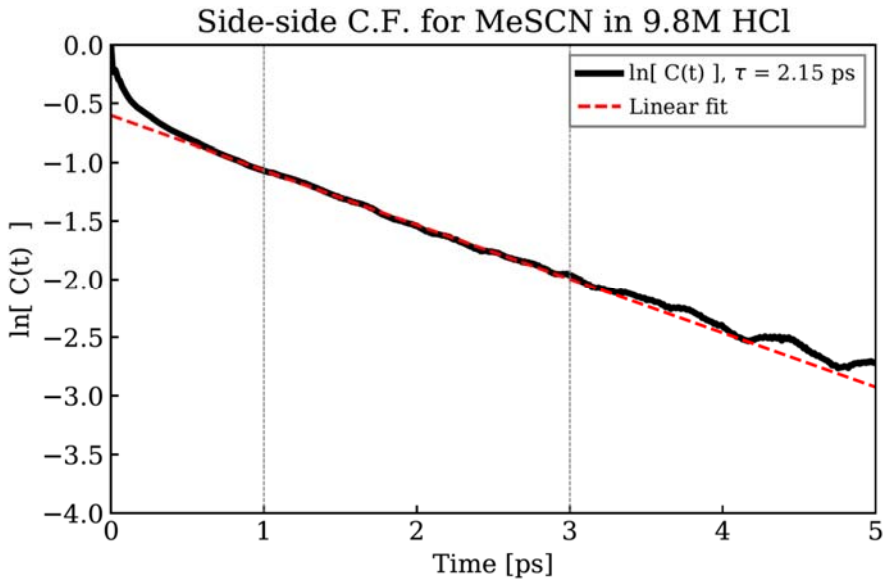

Figure S8. The fit to the logarithm of the side-side correlation function from which the time constant for the exchange process was extracted. We extracted the hydronium-water exchange time scale by performing a fit to the linear region of the logarithm of the correlation function between 1 and 3 ps.

B8. Assigning the transitions: Calculating the percentage of events due to proton transfer vs. percentage due to replacement by H_2O

In the main text, we separate the overall rate of decay from the hydronium-bound state into contributions arising from (i.) replacement by water, (ii.) proton transfer, or (iii.) both at once ("concerted"). When the probe transitions from the hydronium-bound state to the water-bound state in our trajectories, we classified the transition as detailed below.

As discussed in the previous section, a transition has occurred whenever the probe is initially in the hydronium-bound state, defined as when an H* atom is initially within 2.25 Angstroms from the MeSCN nitrogen atom, and then leaves this state. This can occur via three pathways (shown in Fig. 4):

1.) Proton transfer: If, after the transition occurs, the original H* atom remains within the cutoff, but is no longer H*, then we classify the transition as proton transfer.
2.) Water replacement: If the original H* remains H* after the transition, but is no longer within the cutoff distance of 2.25 Angstroms, then we classify the transition as water replacement.
3.) "Concerted": If the original H* atom is no longer within the cutoff *and* no longer is an H* atom, then we classify the transition as "concerted" since both proton transfer and water replacement have occurred simultaneously within the time resolution of our simulations. We note that the definition "concerted" is dependent on the spacing of simulation frames (i.e. both events happened between two frames) which in this case was 2 fs. However, "concerted" events only account for 3% of events and so have minimal effect on the analysis.

Having defined these three mechanisms, we then calculated the proportion of the decay they account for at each time. Starting from the hydronium-bound state, i.e. $h(0)=1$, any transition that occurs at a time t which results in a transition to the water-bound state, i.e. $h(t)=0$, can be uniquely assigned to have occurred by proton transfer (PT), replacement, or a concerted change. Hence one can define the indicator functions $h_{\mathrm{PT}}(t)$, $h_{\mathrm{replacement}}(t)$ and $h_{\mathrm{concerted}}(t)$ which all hold the value 0 whenever $h(t)=1$. When a hydronium unbinding event occurs at a time t and thus $h(t)\rightarrow 0$, it is assigned to one of the three mechanisms and the value of $h_X(t)$, where X is the relevant mechanism, becomes 1. Hence, at any time t:

$$h(t)+h_{\mathrm{PT}}(t)+h_{\mathrm{replacement}}(t)+h_{\mathrm{concerted}}(t)=1$$

i.e. any decay in $h(t)$ from 1 to 0 results in an increment in the indicator for the associated mechanism.

Using the above property of the indicator functions, the total correlation function of the hydronium bound state above can be decomposed as

$$C(t)=\frac{\langle h(0)h(t)\rangle-\langle h\rangle^2}{\langle h\rangle-\langle h\rangle^2}=\frac{\left\langle h(0)\left[1-h_{\mathrm{PT}}(t)-h_{\mathrm{replacement}}(t)-h_{\mathrm{concerted}}(t)\right]\right\rangle-\langle h\rangle^2}{\langle h\rangle-\langle h\rangle^2}$$

$$C(t)=1-\frac{1}{\langle h\rangle-\langle h\rangle^2}\left[\langle h(0)h_{\mathrm{PT}}(t)\rangle+\langle h(0)h_{\mathrm{replacement}}(t)\rangle+\langle h(0)h_{\mathrm{concerted}}(t)\rangle\right]$$

Hence,

$$C(t)=1-\left[C_{\mathrm{PT}}(t)+C_{\mathrm{replacement}}(t)+C_{\mathrm{concerted}}(t)\right]$$

where $C_{\mathrm{PT}}(t)=\frac{\langle h(0)h_{\mathrm{PT}}(t)\rangle}{\langle h\rangle-\langle h\rangle^2}$, $C_{\mathrm{replacement}}(t)=\frac{\langle h(0)h_{\mathrm{replacement}}(t)\rangle}{\langle h\rangle-\langle h\rangle^2}$ and $C_{\mathrm{concerted}}(t)=\frac{\langle h(0)h_{\mathrm{concerted}}(t)\rangle}{\langle h\rangle-\langle h\rangle^2}$.

An important property of the above correlation functions is that all of the decay of $C(t)$ is offset by the other correlation functions, leading to the conservation property

$$C(t)+C_{\mathrm{PT}}(t)+C_{\mathrm{replacement}}(t)+C_{\mathrm{concerted}}(t)=1 \quad .$$

The physical interpretation of $C(t)$ is: what proportion of the decay to its hydronium binding equilibrium average has occurred by time t, given that MeSCN began in a hydronium-bound state at time 0. Hence $C_{\mathrm{PT}}(t)$ can be understood as: what proportion of the decay to its hydronium binding equilibrium average has occurred *via proton transfer* by time t, given that MeSCN began in a hydronium-bound state at time 0. A similar interpretation can be applied to $C_{\mathrm{replacement}}(t)$ or $C_{\mathrm{concerted}}(t)$ where the conversion is due to replacement or a concerted change, respectively. We also note that, should a MeSCN leave the hydronium bound state at time t but return to it at some time t' later (t'>t), then, when this return occurs it no longer contributes to $C_{\mathrm{PT}}(t)$ (or to $C_{\mathrm{replacement}}(t)$ or $C_{\mathrm{concerted}}(t)$ if the event was classified as one of these). This is important as it means that any short time proton "rattling" events only appear in the short time

part of $C_{PT}(t)$ and hence the long time limit of this correlation function *exclusively* counts the proportion of events that lead to the long time decay of $C(t)$. We extracted the proportion of decorrelation that is attributable to proton transfer, water replacement and "concerted" events as the average of the respective curves over the time range 15 – 30 ps, yielding the values 83%, 14% and 3% respectively. The correlation functions are presented below in Fig. S9.

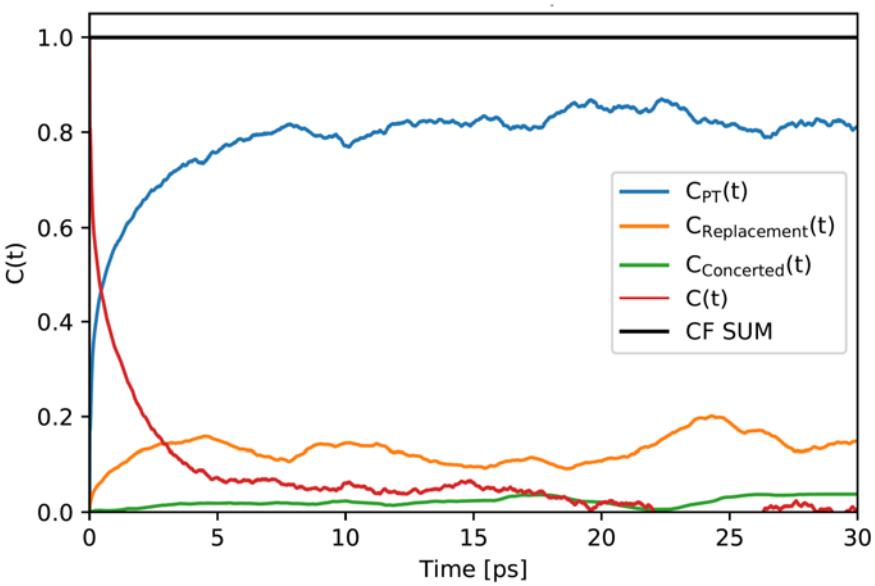

Figure S9. Decomposition of the mechanism of decorrelation of the hydronium bound state. As the hydronium bound state decorrelates (red curve), density accumulates in the proton transfer and water replacement curves as those events are observed. We note that, as detailed above, the sum of the correlation functions ($C(t)$, $C_{PT}(t)$ $C_{replacement}(t)$, $C_{concerted}(t)$.) is 1 at all times (black curve), indicating that all decay in $C(t)$ is exactly offset by increases in the other correlation functions.

B9. Simulations of HCl without the MeSCN probe

In addition to the AIMD simulations of MeSCN in concentrated HCl solution, to assess the effect of the probe on the dynamics we performed AIMD simulations of HCl solutions without the MeSCN probe, ranging in concentration from 0.8 M (one proton defect in a box of 64 water molecules) to 10.5 M. The preparation of these systems followed the same procedure and simulation parameters as detailed previously for systems of 2 M and 4 M HCl[43]. In total, we performed 718 ps, 330 ps, 386 ps, 396 ps, and 177 ps of simulation of 0.8 M, 2 M, 4 M, 8 M, and 10.5 M HCl, respectively. For the 2 M, 4 M, 8 M, and 10.5 M HCl systems, the number of water molecules and HCl pairs in the system were: 106 and 4, 102 and 8, 92 and 16, and 95 and 23,

respectively. The cubic box lengths were 14.905, 14.926, 14.897, and 15.400 Angstroms, respectively.

B10. Calculation of the number of proton leaving pathways

The number of proton leaving pathways referred to in the main text was defined as the average coordination number of the O* oxygen atoms in the simulation. For each acid concentration this coordination number was extracted from the O*-O RDF defining the first coordination shell to end at a distance of 2.88 Angstroms, which was obtained from the minimum in the RDF between the first and second peaks. Fig. S10 shows that as the concentration is increased from 0.8 M to 10.5 M, the running coordination number decreases from 3 to 2.14. This reflects the fact that at higher concentrations, hydronium defects are likely to be solvated partially by chloride. Table S2 gives the number of pathways extracted at each concentration.

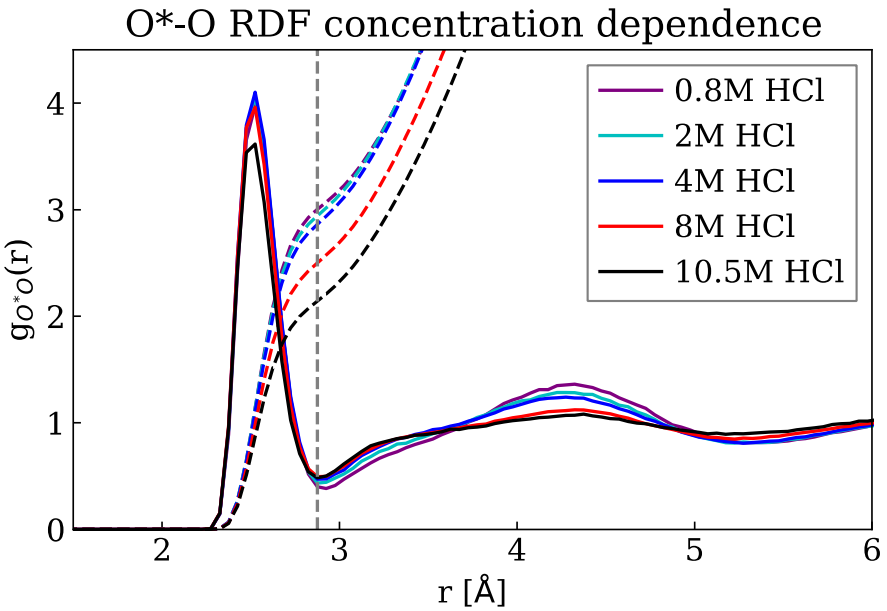

Figure S10. O*-O radial distribution function (RDF) with respect to acid concentration. The vertical dotted grey line is positioned at 2.88 Angstroms, the first minimum in the RDF and the distance at which we extract the number of proton leaving pathways from the running coordination number.

For the MeSCN in 9.8 M HCl system, we extracted the O*-O RDF for the sub-ensemble of O* molecules that are bound to the probe, which is shown in Fig.S11, which yields a value of

1.69 leaving pathways on average. This value is lower than obtained without the probe present since binding of the probe blocks off one of the leaving pathways.

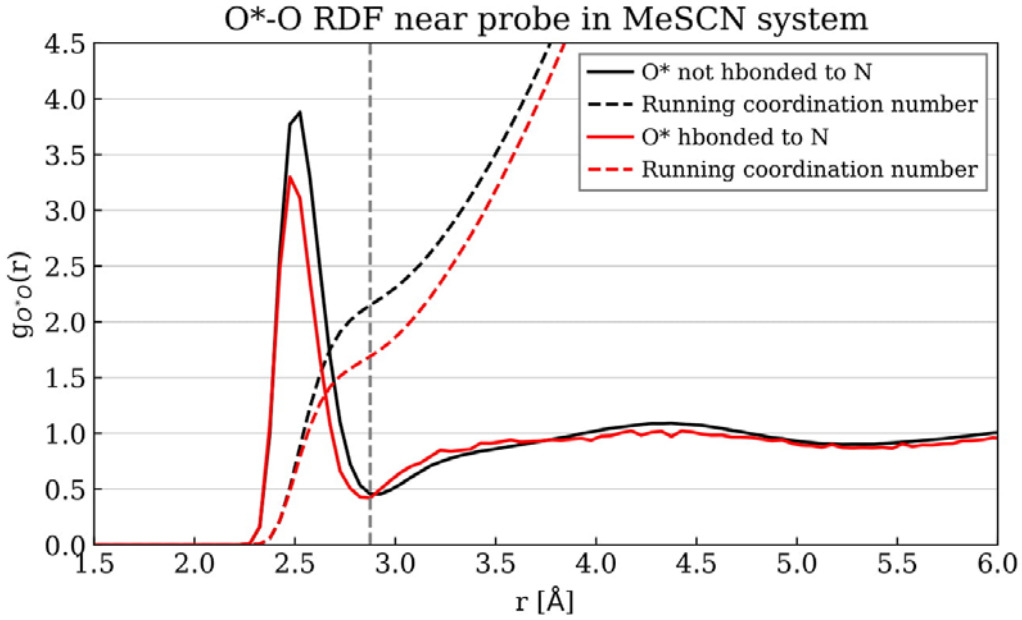

Figure S11. O*-O radial distribution function (RDF) for MeSCN in 9.8 M HCl. The vertical dotted grey line is positioned at 2.88 Angstroms, the first minimum in the RDF and the distance at which we extract the number of proton leaving pathways from the running coordination number. We observe a decrease in the coordination number when looking at the sub-ensemble of O* near the probe, indicating that the probe decreases the number of proton leaving pathways.

Acid concentration [M]	**O* integrated coordination number at r = 2.88 Å.**
0.8	3.0
2.0	2.94
4.0	2.86
8.0	2.50
10.5	2.14

Table S2. Number of proton leaving pathways for each concentration as obtained from the O*-O RDF at each concentration.

B11. Calculation of k_f^{hop} per leaving pathway

To compare the value of k_f obtained from the experiments with the MeSCN probe present to protons in dilute solution, two factors must be taken into account that can be tested using simulations:

1.) **That one can use the proportion of hopping obtained to convert k_f to k_f^{hop}** Here the former is the pseudo first order rate constant for the process of a MeSCN bound to a hydronium to convert to a water and the latter is the rate at which a hydronium bound to MeSCN will transfer a proton to another water. One can convert the former into the latter by multiplication by the proportion of hopping 83% to obtain a value of $k_f^{hop} = 0.010$ ps^{-1} M^{-1}. We can then compare this to the rate obtained by directly calculating the rate at which a hydronium that is bound to a MeSCN converts to a water molecule, which is 0.0089 ps^{-1} M^{-1}. Relative to the value obtained directly, the value obtained by using k_f and the proportion of hopping differs by 12% which is well within the statistical error bars of both rates. This suggests that the approach used to convert the experimental k_f to k_f^{hop} in the main text works well when applied to the simulation data where the rate can also be extracted directly.

2.) **That the difference in proton hopping rates k_f^{hop} between protons at high and low concentration can be accounted for by the different number of proton leaving pathways from the hydronium defect.** To address this we simulated HCl solutions ranging in concentration from 0.8 M to 10.5 M (the specific concentrations simulated are provided in Supplementary Materials (SM) B9). At each concentration we extracted k_f^{hop} by first calculating the rate of decay of the O* correlation function (shown in Fig. S12), which is defined as in SM B7, but with $h(t)$=1 when a given O atom in the simulation is triply coordinated and $h(t)$=0 otherwise[45]. The slope of the logarithm of resulting correlation function (extracted from linear fits to the logarithm of the correlation functions between 1.0 ps and 3.0 ps) gives k_{HW}^{hop} which can be converted into the pseudo first order hopping rate using,

$$k_f^{hop} = k_{HW}^{hop}\left[\mathrm{H_2O}\right]^{-1}$$

This gives the values in Table S3. As described in the previous section, we obtained the number of proton leaving pathways (shown in Table S2) from the O*-O RDF for each system. We then

calculated the k_f^{hop} per leaving pathway by dividing the rates in Table S3 by the number of leaving pathways in Table S2 at each concentration to yield the values shown in Table S3. While k_f^{hop} changes noticeably with changing concentration, k_f^{hop} per leaving pathway does not change. This justifies the application of the factor of 3.0/1.69 to k_f^{hop} obtained from the experiment to account for the differing number of leaving pathways available to protons in dilute solution vs protons belonging to hydronium molecules near MeSCN in solution.

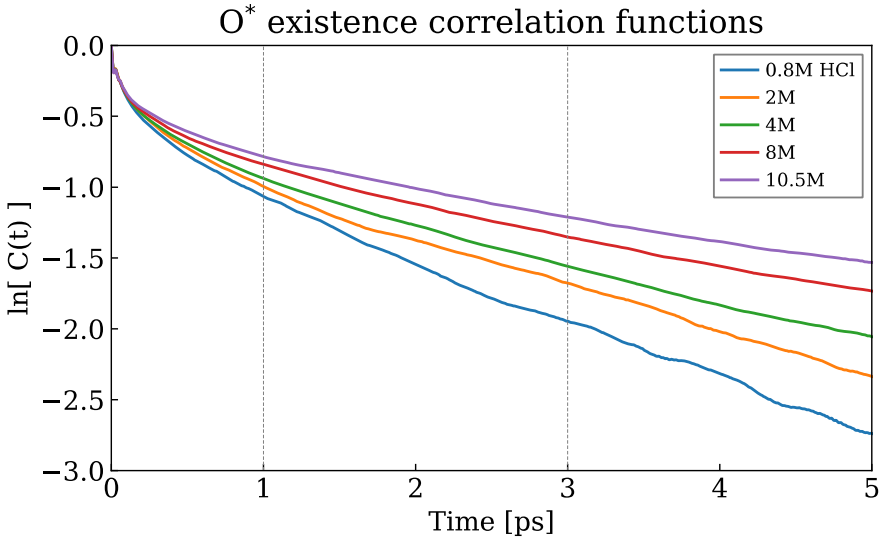

Figure S12. Natural logarithms of the O* existence correlation functions for HCl solutions of various concentrations. While the beginnings of these correlation functions (<0.5 ps) exhibit an initial rapid decay due to proton rattling, the longer time scale decay occurs due to proton transfer. We extracted k_{eq} from linear fits to the logarithm of the correlation functions between 1.0 ps and 3.0 ps.

Acid concentration [M]	k_{HW}^{hop} **[ps^{-1}]**	**[H_2O] [M]**	k_f^{hop} **[ps^{-1} M^{-1}]**	k_f^{hop} **per pathway [ps^{-1} M^{-1}]**
0.8	0.449	54.6	0.00823	0.0027
2.0	0.311	51.2	0.00607	0.0021
4.0	0.281	46.9	0.00599	0.0021
8.0	0.208	38.2	0.00544	0.0022
10.5	0.161	32.7	0.00493	0.0023

Table S3. k_f^{hop} obtained from O* existence correlation functions

References – Supplementary Information

(1) Zheng, J. R.; Kwak, K. W.; Xie, J.; Fayer, M. D., Ultrafast carbon-carbon single-bond rotational isomerization in room-temperature solution, *Science* **2006**, *313*, 1951-1955.

(2) Ishikawa, H.; Kwak, K.; Chung, J. K.; Kim, S.; Fayer, M. D., Direct observation of fast protein conformational switching, *Proc. Natl. Acad. Sci. U.S.A.* **2008**, *105*, 8619-8624.

(3) Kwak, K.; Zheng, J.; Cang, H.; Fayer, M. D., Ultrafast 2D IR Vibrational Echo Chemical Exchange Experiments and Theory, *J. Phys. Chem. B* **2006**, *110*, 19998-20013.

(4) Ji, M.; Odelius, M.; Gaffney, K. J., Large Angular Jump Mechanism Observed for Hydrogen Bond Exchange in Aqueous Perchlorate Solution, *Science* **2010**, *328*, 1003-1005.

(5) Tan, H.-S.; Piletic, I. R.; Fayer, M. D., Polarization selective spectroscopy experiments: Methodology and pitfalls, *J. Op. Soc. Am. B: Optical Physics* **2005**, *22*, 2009-2017.

(6) Yuan, R. F.; Yan, C.; Nishida, J.; Fayer, M. D., Dynamics in a Water Interfacial Boundary Layer Investigated with IR Polarization-Selective Pump-Probe Experiments, *J. Phys. Chem. B* **2017**, *121*, 4530-4537.

(7) Steinel, T.; Asbury, J. B.; Zheng, J. R.; Fayer, M. D., Watching hydrogen bonds break: A transient absorption study of water, *J. Phys. Chem. A* **2004**, *108*, 10957-10964.

(8) Giammanco, C. H.; Wong, D. B.; Fayer, M. D., Water Dynamics in Divalent and Monovalent Concentrated Salt Solutions, *J. Phys. Chem. B* **2012**, *116*, 13781-13792.

(9) Kwak, K.; Rosenfeld, D. E.; Fayer, M. D., Taking apart the two-dimensional infrared vibrational echo spectra: More information and elimination of distortions, *J. Chem. Phys.* **2008**, *128*, 204505.

(10) Kwak, K.; Park, S.; Finkelstein, I. J.; Fayer, M. D., Frequency-Frequency Correlation Functions and Apodization in 2D-IR Vibrational Echo Spectroscopy, a New Approach, *Journal of Chemical Physics* **2007**, *127*, 124503.

(11) Giammanco, C. H.; Kramer, P. L.; Fayer, M. D., Dynamics of Dihydrogen Bonding in Aqueous Solutions of Sodium Borohydride, *J. Phys. Chem. B* **2015**, *119*, 3546-3559.

(12) Fenn, E. E.; Fayer, M. D., Extracting 2D IR Frequency-Frequency Correlation Functions from Two Component Systems, *J. Chem. Phys.* **2011**, *135*, 07450.

(13) Kapil, V.; Rossi, M.; Marsalek, O.; Petraglia, R.; Litman, Y.; Spura, T.; Cheng, B.; Cuzzocrea, A.; Meißner, R. H.; Wilkins, D. M.; Helfrecht, B. A.; Juda, P.; Bienvenue, S. P.; Fang, W.; Kessler, J.; Poltavsky, I.; Vandenbrande, S.; Wieme, J.; Corminboeuf, C.; Kühne, T. D.; Manolopoulos, D. E.; Markland, T. E.; Richardson, J. O.; Tkatchenko, A.; Tribello, G. A.; Van Speybroeck, V.; Ceriotti, M., i-PI 2.0: A universal force engine for advanced molecular simulations, *Comput. Phys. Comm.* **2019**, *236*, 214-223.

(14) Ceriotti, M.; More, J.; Manolopoulos, D. E., i-PI: A Python interface for ab initio path integral molecular dynamics simulations, *Comput. Phys. Comm.* **2014**, *185*, 1019-1026.

(15) Tuckerman, M.; Berne, B. J.; Martyna, G. J., Reversible Multiple Time Scale Molecular-Dynamics, *J.Chem. Phys.* **1992**, *97*, 1990-2001.

(16) Wang, J. M.; Wolf, R. M.; Caldwell, J. W.; Kollman, P. A.; Case, D. A., Development and testing of a general amber force field, *J. Comput. Chem.* **2004**, *25*, 1157-1174.

(17) Wang, J. M.; Wang, W.; Kollman, P. A.; Case, D. A., Automatic atom type and bond type perception in molecular mechanical calculations, *J. Mol. Graph. Model.* **2006**, *25*, 247-260.

(18) Smith, D. E.; Dang, L. X., Computer-Simulations of Nacl Association in Polarizable Water, *J. Chem. Phys.* **1994**, *100*, 3757-3766.

(19) Wang, L. P.; Martinez, T. J.; Pande, V. S., Building Force Fields: An Automatic, Systematic, and Reproducible Approach, *J. Phys. Chem. Lett.* **2014**, *5*, 1885-1891.

(20) Eastman, P.; Pande, V. S., Efficient Nonbonded Interactions for Molecular Dynamics on a Graphics Processing Unit, *J. Comput. Chem.* **2010**, *31*, 1268-1272.

(21) Eastman, P.; Pande, V. S., OpenMM: A Hardware-Independent Framework for Molecular Simulations, *Comput. Sci. Eng.* **2010**, *12*, 34-39.

(22) Eastman, P.; Swails, J.; Chodera, J. D.; McGibbon, R. T.; Zhao, Y. T.; Beauchamp, K. A.; Wang, L. P.; Simmonett, A. C.; Harrigan, M. P.; Stern, C. D.; Wiewiora, R. P.; Brooks, B. R.; Pande, V. S., OpenMM 7: Rapid development of high performance algorithms for molecular dynamics, *PLoS. Comput. Biol.* **2017**, *13*, e1005659.

(23) Friedrichs, M. S.; Eastman, P.; Vaidyanathan, V.; Houston, M.; Legrand, S.; Beberg, A. L.; Ensign, D. L.; Bruns, C. M.; Pande, V. S., Accelerating Molecular Dynamic Simulation on Graphics Processing Units, *J. Comput. Chem.* **2009**, *30*, 864-872.

(24) Galib, M.; Duignan, T. T.; Misteli, Y.; Baer, M. D.; Schenter, G. K.; Hutter, J.; Mundy, C. J., Mass density fluctuations in quantum and classical descriptions of liquid water, *J. Chem. Phys.* **2017**, *146*, 244501

(25) VandeVondele, J.; Krack, M.; Mohamed, F.; Parrinello, M.; Chassaing, T.; Hutter, J., QUICKSTEP: Fast and accurate density functional calculations using a mixed Gaussian and plane waves approach, *Comput. Phys. Comm.* **2005**, *167*, 103-128.

(26) Hutter, J.; Iannuzzi, M.; Schiffmann, F.; VandeVondele, J., CP2K: atomistic simulations of condensed matter systems, *Wiley Interdisciplinary Reviews-Computational Molecular Science* **2014**, *4*, 15-25.

(27) Perdew, J. P.; Burke, K.; Ernzerhof, M., Generalized gradient approximation made simple, *Phys. Rev. Lett.* **1996**, *77*, 3865-3868.

(28) Zhang, Y. K.; Yang, W. T., Comment on "Generalized gradient approximation made simple", *Phys. Rev. Lett.* **1998**, *80*, 890-890.

(29) Grimme, S.; Antony, J.; Ehrlich, S.; Krieg, H., A consistent and accurate ab initio parametrization of density functional dispersion correction (DFT-D) for the 94 elements H-Pu, *J. Chem. Phys.* **2010**, *132*, 154104.

(30) Goedecker, S.; Teter, M.; Hutter, J., Separable dual-space Gaussian pseudopotentials, *Phys. Rev. B.* **1996**, *54*, 1703-1710.

(31) Lippert, G.; Hutter, J.; Parrinello, M., A hybrid Gaussian and plane wave density functional scheme, *Mol. Phys.* **1997**, *92*, 477-487.

(32) VandeVondele, J.; Hutter, J., An efficient orbital transformation method for electronic structure calculations, *J. Chem. Phys.* **2003**, *118*, 4365-4369.

(33) Kolafa, J., Time-reversible always stable predictor-corrector method for molecular dynamics of polarizable molecules, *J. Comput. Chem.* **2004**, *25*, 335-342.

(34) Kuhne, T. D.; Krack, M.; Mohamed, F. R.; Parrinello, M., Efficient and accurate Car-Parrinello-like approach to Born-Oppenheimer molecular dynamics, *Phys. Rev. Lett.* **2007**, *98*, 1-4.

(35) Marsalek, O.; Markland, T. E., Ab initio molecular dynamics with nuclear quantum effects at classical cost: Ring polymer contraction for density functional theory, *J. Chem. Phys.* **2016**, *144*, 054112.

(36) Luehr, N.; Markland, T. E.; Martinez, T. J., Multiple time step integrators in ab initio molecular dynamics, *J. Chem. Phys.* **2014**, *140*, 084116.

(37) Gaus, M.; Cui, Q. A.; Elstner, M., DFTB3: Extension of the Self-Consistent-Charge Density-Functional Tight-Binding Method (SCC-DFTB), *J. Chem. Theory. Comput.* **2011**, *7*, 931-948.

(38) Aradi, B.; Hourahine, B.; Frauenheim, T., DFTB+, a sparse matrix-based implementation of the DFTB method, *J. Phys. Chem. A* **2007**, *111*, 5678-5684.

(39) Gaus, M.; Goez, A.; Elstner, M., Parametrization and Benchmark of DFTB3 for Organic Molecules, *J. Chem. Theory. Comput.* **2013**, *9*, 338-354.

(40) Zhechkov, L.; Heine, T.; Patchkovskii, S.; Seifert, G.; Duarte, H. A., An efficient a Posteriori treatment for dispersion interaction in density-functional-based tight binding, *J. Chem. Theory. Comput.* **2005**, *1*, 841-847.

(41) Rappe, A. K.; Casewit, C. J.; Colwell, K. S.; Goddard, W. A.; Skiff, W. M., UFF, a Full Periodic-Table Force-Field for Molecular Mechanics and Molecular-Dynamics Simulations, *J. Am. Chem. Soc.* **1992**, *114*, 10024-10035.

(42) Habershon, S.; Markland, T. E.; Manolopoulos, D. E., Competing quantum effects in the dynamics of a flexible water model, *J. Chem. Phys.* **2009**, *131*, 024501

(43) Napoli, J. A.; Marsalek, O.; Markland, T. E., Decoding the spectroscopic features and time scales of aqueous proton defects, *J. Chem. Phys.* **2018**, *148*, 222833.

(44) Marsalek, O.; Markland, T. E., Quantum Dynamics and Spectroscopy of Ab Initio Liquid Water: The Interplay of Nuclear and Electronic Quantum Effects, *J. Phys. Chem. Lett.* **2017**, *8*, 1545-1551.

(45) Frenkel, D.; Smit, B. In *Understanding Molecular Simulation (Second Edition)*; Frenkel, D., Smit, B., Eds.; Academic Press: San Diego, 2002, p 431-464.